



University of
Massachusetts
Amherst

Luminous Infrared Galaxies With The Submillimeter Array. Ii. Comparing The Co (3-2) Sizes And Luminosities Of Local And High-redshift Luminous Infrared Galaxies

Item Type	Article
Authors	Iono, D;Wilson, CD;Yun, Min;Baker, AJ;Petitas, GR;Peck, AB;Krips, M;Cox, TJ;Matsushita, S;Mihos, JC;Pihlstrom, Y
DOI	10.1088/0004-637X/695/2/1537
Download date	2026-05-17 11:32:34
Link to Item	https://hdl.handle.net/20.500.14394/2757

LUMINOUS INFRARED GALAXIES WITH THE SUBMILLIMETER ARRAY: II. COMPARING THE CO (3–2) SIZES AND LUMINOSITIES OF LOCAL AND HIGH-REDSHIFT LUMINOUS INFRARED GALAXIES

DAISUKE IONO^{1,2}, CHRISTINE D. WILSON³, MIN S. YUN⁴, ANDREW J. BAKER⁵, GLEN R. PETITPAS⁶, ALISON B. PECK⁷, MELANIE KRIPS⁶, T. J. COX⁶, SATOKI MATSUSHITA⁸, J. CHRISTOPHER MIHOS⁹, YLVA PIHLSTROM¹⁰

Draft version February 1, 2009

ABSTRACT

We present a detailed comparison of the CO (3–2) emitting molecular gas between a local sample of luminous infrared galaxies (U/LIRGs) and a high redshift sample that comprises submm selected galaxies (SMGs), quasars, and Lyman Break Galaxies (LBGs). The U/LIRG sample consists of our recent CO (3–2) survey using the Submillimeter Array while the CO (3–2) data for the high redshift population are obtained from the literature. We find that the $L'_{\text{CO}(3-2)}$ and L_{FIR} relation is correlated over five orders of magnitude, which suggests that the molecular gas traced in CO (3–2) emission is a robust tracer of dusty star formation activity. The near unity slope of 0.93 ± 0.03 obtained from a fit to this relation suggests that the star formation efficiency is constant to within a factor of two across different types of galaxies residing in vastly different epochs. The CO (3–2) size measurements suggest that the molecular gas disks in local U/LIRGs (0.3 – 3.1 kpc) are much more compact than the SMGs (3 – 16 kpc), and that the size scales of SMGs are comparable to the nuclear separation (5 – 40 kpc) of the widely separated nuclei of U/LIRGs in our sample. We argue from these results that the SMGs studied here are predominantly intermediate stage mergers, and that the wider line-widths arise from the violent merger of two massive gas-rich galaxies taking place deep in a massive halo potential.

Subject headings: galaxies: formation, galaxies: starburst, cosmology: observations, galaxies: high redshift, submillimeter

1. INTRODUCTION

Ultra/Luminous Infrared Galaxies (U/LIRGs) are sources that emit large amounts of flux in the far-infrared (FIR) bands, with FIR luminosities in the range $10^{11-12} L_{\odot}$ (for LIRGs) or even larger ($> 10^{12} L_{\odot}$ for ULIRGs) (see reviews by Sanders & Mirabel 1996; Lonsdale, Farrah & Smith 2006). These galaxies were discovered by the *Infrared Astronomical Satellite* (IRAS) to be fairly rare in the local universe, but show significant increase as a function of redshift (Hacking, Houck & Condon 1987). Followup optical studies of nearby U/LIRGs have revealed that the morphologies of a significant fraction of them resemble interacting/merging systems (Armus, Heckman & Miley 1987), mostly powered by starbursts with increasing contribution from Active Galactic

Nuclei (AGN) for IR-brighter galaxies (Kim, Veilleux, & Sanders 1998). These galaxies harbor large amounts of molecular gas (Sanders et al. 1986) that is often concentrated near the compact nuclear regions (Downes & Solomon 1998; Bryant & Scoville 1999). These observational findings were analyzed in conjunction with numerical simulations that date back as far as the 1970's (Toomre & Toomre 1972), further advanced with the inclusion of gas dynamics and star formation recipes in the 1990's (Barnes & Hernquist 1996; Mihos & Hernquist 1996) and with realistic feedback mechanisms implemented in the 2000's (Springel, Yoshida & White 2001; Springel, Di Matteo & Hernquist 2005; Cox et al. 2006). As a result, it is widely believed that tidally triggered gas compression and subsequent starbursts (and/or AGN fueling) heat the surrounding dust, are reprocessed into far-infrared emission, and result in the intriguing U/LIRG phenomenon we observe in the local as well as the high redshift universe.

Since the late 1990's, with the advent of sensitive mm/submm bolometer cameras mounted on single dish telescopes, observations of the blank sky have revealed the ubiquitous presence of unresolved sources that appear to account for a substantial fraction of the total infrared background radiation (see Lagache, Puget, & Dole 2005, for a review). By using the correlation between radio and FIR (Condon 1992), interferometric radio observations toward these sources and subsequent followup optical spectroscopy have provided substantial evidence that the origin of this emission is dusty star-forming galaxies that reside at $z \geq 2$ (Chapman et al. 2004b). The FIR luminosities and molecular gas properties in these submillimeter selected galaxies (SMGs)

¹ Institute of Astronomy, The University of Tokyo, 2-21-1 Otsu, Mitaka, Tokyo 181-0015, Japan

² Current address; National Radio Observatory, NAOJ, Minamimaki, Minamisaku, Nagano, 384-1305, Japan; d.iono@nao.ac.jp

³ Department of Physics and Astronomy, McMaster University, Hamilton, ON L8S 4M1, Canada

⁴ Department of Astronomy, University of Massachusetts, Amherst, MA 01003

⁵ Department of Physics and Astronomy, Rutgers, the State University of New Jersey, 136 Frelinghuysen Road, Piscataway, NJ 08854-8019

⁶ Harvard-Smithsonian Center for Astrophysics, Cambridge, MA 02138

⁷ Joint ALMA Office, Avda El Golf 40, piso 18, Santiago 7550108 Chile

⁸ Academia Sinica Institute of Astronomy and Astrophysics, Taipei 106, Taiwan

⁹ Department of Astronomy, Case Western Reserve University, 10900 Euclid Avenue, Cleveland, OH 44106

¹⁰ Department of Physics and Astronomy, University of New Mexico, Albuquerque, NM 87131

are generally an order of magnitude larger than the local U/LIRGs (Greve et al. 2005; Tacconi et al. 2006, 2008). While the FIR luminosities in local U/LIRGs appear to be powered primarily by starbursts and in some cases a central AGN (e.g. Genzel et al. 1998), recent studies have suggested that the AGN contribution to the FIR luminosity is negligible in the high redshift SMGs (Pope et al. 2006, 2008).

It has long been proposed that U/LIRGs and quasars are linked through dynamical evolution of the host systems, likely by a merger event (Sanders et al. 1988a; Hopkins et al. 2005). The initial stages of the merger could be dominated by dusty starbursts (i.e. U/LIRGs and SMGs), until the central nuclear activity is stimulated by massive gas accretion. When the cold gas is consumed either by starbursts or accretion onto the central AGN, the quasar may become visible as intervening dusty high column density material along our line of sight clears away. This merger evolution scenario is partially supported by recent deep and high-resolution imaging of quasar host galaxies (Dunlop et al. 2003; Sanchez et al. 2004; Veilleux et al. 2006; Zakamska et al. 2006), where morphological signatures of interactions/mergers and spheroidal systems are evident.

Since the important fuel of the activity, whether it be starbursts or AGN, is warm and dense gas, a large sample of molecular line data in IR bright galaxies and quasars at different epochs is needed. This data set allows us to test whether the evolutionary scenario is consistent with observations in the local universe, and then to test whether it holds true at high redshifts. Single dish and interferometric observations of the CO (1–0) emission in local U/LIRGs have been carried out previously, providing significant evidence that the amount of gas in these systems is massive, and highly concentrated in the nucleus (e.g. Downes & Solomon 1998). Similar observations have been conducted in CO emission of the redshifted high- J transition lines from SMGs/quasars (see Solomon & vanden Bout 2005, for a review), but these observations are difficult due to the requirement of a precise knowledge of the redshift and the lack of sensitivity at mm/submm bands, and therefore the sample is biased toward the brightest (or gravitationally lensed) sources.

The majority of the molecular gas detections in the bright SMGs/quasars thus far from $z \gtrsim 2$ sources are CO (3–2) (or higher J) line redshifted to the mm bands. However, directly comparing the properties of the CO (3–2) emission in the SMGs/quasars with the CO (1–0) emission in the local galaxies can be significantly biased by excitation effects¹¹. Thus, to properly assess the characteristics of gas in U/LIRGs and high redshift SMGs/quasars, a thorough comparison of a single J transition emission line is needed. We have carried out a program at the Submillimeter Array (SMA)¹² (Ho, Moran & Lo 2004) to observe 14 U/LIRGs in the local universe in the CO (3–2) and CO (2–1) lines (Wilson et al. 2008, Paper I hereafter). Because the critical density of CO (3–2) emission is relatively high, it is considered as an impor-

tant tracer of the physical condition of the star forming gas and the associated kinematics. This common belief, however, has not been fully tested observationally because of the lack of high resolution observations of nearby and distant sources. Recent high resolution studies of local U/LIRGs show, in some cases, that the distribution and the peak of the CO (3–2) emission could be different from the lower transition CO (e.g. Iono et al. 2004).

In order to conduct an analysis that is not biased by excitation effects, we present a detailed comparison of the CO (3–2) emitting molecular gas between a local sample of U/LIRGs and a high redshift sample that comprises SMGs, quasars, and two Lyman Break Galaxies (LBGs) that have been recently detected in CO (3–2). We also include CO (3–2) data from a sample of local quiescent galaxies in some of the analyses. The U/LIRG sample consists of our recent CO (3–2) survey using the SMA (Paper I) while the CO (3–2) data for the high redshift and local quiescent galaxies are obtained from the literature.

In §2, we present the sample data and the formalism for deriving the relevant parameters. In §3, we investigate the correlation between CO (3–2) and FIR luminosities in a variety of sources, and offer possible interpretations of the derived slope and the scatter seen in the correlation. We compare the CO (3–2) source size in different sources and offer clues to the merger stage of SMGs and quasars in §4. We present our conclusions in §5. We adopt $H_0 = 70 \text{ km s}^{-1} \text{ Mpc}^{-1}$, $\Omega_M = 0.3$, $\Omega_\Lambda = 0.7$ for all of the analysis throughout this paper.

2. SAMPLE DATA AND DERIVED QUANTITIES

Observational details and the properties of the local U/LIRG data are described in Paper I. The U/LIRG sample consists of 14 sources, of which six are interacting/merging galaxy pairs whose nuclei are resolved into multiple components (“pre-coalescence” mergers), and eight are mergers whose nuclei are unresolved even with space-based optical images (“post-coalescence” mergers). For the remainder of the paper, the local infrared bright galaxies with $L_{\text{FIR}} > 10^{12} L_\odot$ are referred to as ULIRGs, whereas galaxies with $L_{\text{FIR}} < 10^{12} L_\odot$ are referred to as LIRGs. The term U/LIRG is used when referring to the entire sample presented in Paper I, regardless of the FIR luminosity.

Interferometric CO (3–2) data toward SMGs were obtained from published results in Neri et al. (2003), Sheth et al. (2004), Greve et al. (2005), Tacconi et al. (2006, 2008) and Knudsen et al. (2008). A few sources that were observed in Greve et al. (2005) were also observed by Tacconi et al. (2006) at higher angular resolution, and we adopt the latter for our analysis. In addition, CO (3–2) emission in MIPS-J1428 (Iono et al. 2006a), a submm bright HyLIRG (Hyper Luminous InfraRed Galaxy; $L_{\text{FIR}} > 10^{13} L_\odot$) at $z = 1.3$, was also included in our SMG sample. The CO (3–2) data for the quasars were compiled from Hainline et al. (2004), Walter et al. (2004), Solomon & vanden Bout (2005), and Coppin et al. (2008). The two CO (3–2) detected LBGs, MS 1512-cB58 (cB58 hereafter) and J213512-010143 (a.k.a. the “cosmic eye”, J213512 hereafter), were obtained from Baker et al. (2004) and Coppin et al. (2007), respectively.

The far infrared luminosities (L_{FIR}) are obtained from the IRAS Revised Bright Galaxy Sample (BGS) (Sanders

¹¹ $T_{ex} = 33 \text{ K}$ and $n_{crit} = 3.6 \times 10^4 \text{ cm}^{-3}$ for CO (3–2) whereas $T_{ex} = 6 \text{ K}$ and $n_{crit} = 2.2 \times 10^3 \text{ cm}^{-3}$ for CO (1–0)

¹² The Submillimeter Array is a joint project between the Smithsonian Astrophysical Observatory and the Academia Sinica Institute of Astronomy and Astrophysics, and is funded by the Smithsonian Institution and the Academia Sinica.

et al. 2003) for all of the U/LIRGs. The L_{FIR} of SMGs/quasars are derived by fitting a theoretical starburst spectral energy distribution (SED) (Efstathiou, Rowan-Robinson, & Siebenmorgen 2000) to the observed FIR to radio flux densities (Yun & Carilli 2002). The same SEDs were used to compute the L_{FIR} of the three local ULIRGs in our sample, and we found that they are consistent with the Sanders et al. (2003) values to within $< 50\%$. The L_{FIR} of the LBGs are obtained from Baker et al. (2004) and Coppin et al. (2007). The sample sources along with various physical properties used in this study are presented in Table 1.

We derive the following physical properties for the analysis of this paper. The derived physical properties of all of the sources are presented in Table 2.

(1) The CO (3–2) luminosity, $L'_{\text{CO}(3-2)}$ [$\text{K km s}^{-1} \text{pc}^2$], is derived using

$$L'_{\text{CO}(3-2)} = 3.25 \times 10^7 S_{\text{CO}(3-2)} \nu_{\text{obs}}^{-2} (1+z)^{-3} D_L^2. \quad (1)$$

where $S_{\text{CO}(3-2)}$ is the integrated CO(3–2) intensity in Jy km s^{-1} , ν_{obs} is the observed frequency in GHz, D_L is the luminosity distance in Mpc, and z is the redshift of the source (Solomon & vanden Bout 2005).

(2) The full width at half maximum (FWHM) of the CO (3–2) line are estimated using the integrated spectra shown in Fig. 25–29 of Paper I, and obtained from the published results for the SMGs, quasars, and LBGs.

(3) The source sizes of U/LIRGs are the deconvolved FWHM diameters derived by fitting a 2 dimensional Gaussian to the CO (3–2) integrated intensity maps. When the deconvolution failed in some of the sources (mainly due to low S/N), the major and minor FWHM axes obtained from the Gaussian fits in the image domain are given as upper limits to the source size. All of the U/LIRGs are resolved with the SMA beam, except for IRAS 17208-0014 whose deconvolution produces a point source. However, visual inspection of its integrated intensity map in Figure 2 of Paper I suggests that the CO (3–2) emission appears to have a bright compact component, as well as a resolved extended structure.

The published sizes are used for the 6 SMGs that are resolved by the interferometer. Most of the quasars are unresolved except for SDSS J1148+5251, IRAS F10214+4724, and Cloverleaf. High angular resolution VLA observations (Walter et al. 2004) have successfully resolved the structure in the $z = 6.4$ quasar SDSS J1148+5251, whereas OVRO observations (Yun et al. 1997) in conjunction with a lensing model have inferred a source size of $0''.3$ for the highly lensed $z = 2.6$ quasar Cloverleaf. For the remaining unresolved SMGs, quasars, and LBGs, the minor axis of the beam (FWHM) is used as an upper limit to the source size.

Because the physical resolution of the high redshift population is worse than the local LIRGs, some of the widely separated sources that are resolved with the SMA may not be resolved using $0''.8$ resolution when they are placed at $z = 2$. We have tested this by convolving the CO (3–2) images of all of the widely separated pairs with $0''.8$ (~ 8 kpc at $z = 2$) resolution, and found that all the galaxies are clearly resolved into multiple components except for Arp 299, which is only marginally resolved.

(4) The star formation efficiency (SFE), $L_{\text{FIR}}/L'_{\text{CO}(3-2)}$, is derived by taking the ratio be-

tween FIR luminosity and CO (3–2) luminosity. The ratio between FIR luminosity and molecular gas mass (i.e. $L_{\text{FIR}}/M_{\text{H}_2}$) is often used to infer the SFE of a galaxy, but we opted to use the luminosity ratio ($L_{\text{FIR}}/L'_{\text{CO}(3-2)}$) in this study to avoid introducing additional ambiguities through variation and uncertainties pertaining to the conversion from $L'_{\text{CO}(3-2)}$ to M_{H_2} .

We caution that the CO (3–2) properties at low and high redshifts are generally lower limits for the following reasons. In synthesis imaging, incomplete uv coverage results in decreasing sensitivity to extended structure. While the SMA observations are sensitive to structure with size scales of $\lesssim 12'' - 16''$ (7 – 10 kpc on average for these galaxies), the missing flux calculated by comparing to single dish data is 2 – 66% (Paper I). Thus the diffuse and extended CO (3–2) emission would be undetected in the SMA observations, and the values derived in this paper are lower limits to the physical quantities intrinsic to the source. On the other hand, observations of high redshift galaxies are limited in both sensitivity and angular resolution. The relatively coarse angular (physical) resolution of $\lesssim 0''.8$ (~ 6 kpc) allows us to analyze images that do not suffer significantly from the missing-flux problem. However, the high redshift population suffers from limited sensitivity (with mass sensitivity of $\sim 10^{10} M_{\odot}$), and any extended CO (3–2) emission could be buried in the noise. Therefore, the physical quantities derived here from CO (3–2) data for both the low and high redshift populations are likely lower limits.

3. THE CO (3–2) LUMINOSITY AND THE STAR FORMATION EFFICIENCY

The luminosity of the CO (3–2) emission line can be a direct measure of the amount of dense molecular gas fueling nuclear (or extended) star formation and/or the central AGN. The average CO (3–2) luminosities ($L'_{\text{CO}(3-2)}$) derived in U/LIRGs, SMGs, and quasars are $(2.6 \pm 0.5) \times 10^9$, $(4.4 \pm 1.1) \times 10^{10}$ and $(5.0 \pm 1.0) \times 10^{10} \text{ K km s}^{-1} \text{pc}^2$, respectively. The $L'_{\text{CO}(3-2)}$ for the two LBGs are 4.4×10^8 and $2.9 \times 10^9 \text{ K km s}^{-1} \text{pc}^2$ for cB58 and J213512, respectively. The average CO (3–2) luminosity in the U/LIRGs is more than an order of magnitude lower than in the SMGs and quasars, but comparable to the two LBGs. Under the assumption that the powering source of the large L_{FIR} is mostly from starbursts (see §3.1), the comparison between $L'_{\text{CO}(3-2)}$ and L_{FIR} relates the amount of available dense molecular gas to the amount of current massive star formation traced in FIR dust emission. This analysis assumes an environment where the gas is sufficiently dense and warm to thermally (or radiatively) populate the $J=3$ rotational energy level of carbon monoxide, and that the gas and dust are coupled spatially. We investigate the relation between $L'_{\text{CO}(3-2)}$ and L_{FIR} in the following subsection.

3.1. The $L'_{\text{CO}(3-2)} - L_{\text{FIR}}$ Relation

In Figure 1 (*left*), we compare the CO (3–2) line luminosity with the FIR luminosity for all four sample populations. In addition, we have plotted the same luminosity relation for a sample of local galaxies published in Mauersberger et al. (1999) and Komugi et al. (2007) to

increase the luminosity range. The $L'_{\text{CO}(3-2)} - L_{\text{FIR}}$ relation including all four populations (and local galaxies) is correlated over five orders of magnitude in luminosity, which suggests that the molecular gas seen in CO (3–2) emission is a robust tracer of star formation activity. A least-squares fit of the form $\log L'_{\text{CO}(3-2)} = \alpha \log L_{\text{FIR}} + \beta$ gives $\alpha = (0.93 \pm 0.03)$ and $\beta = (-1.50 \pm 0.33)$. Excluding the local galaxies or the quasars, which may have significant dust heating due to the central AGN, does not change the slope with significance. One potential concern here is that the large range in distance may artificially produce a correlation in log-log space. To check whether the correlation seen here is statistically robust, we employed the partial Kendall τ -coefficient with censored data (Akritas & Siebert 1996) where we used the luminosity distance as a test variable. This analysis yields a probability of 7.3×10^{-5} that these two variables will produce a false correlation after the effect of distance is removed, providing solid statistical evidence of correlation in logarithmic space.

The near unity slope derived from the $L_{\text{FIR}} - L'_{\text{CO}(3-2)}$ relation suggests that the efficiency of converting CO (3–2) emitting molecular gas to massive stars (i.e. SFE) is, within a factor of two (i.e. from the standard deviation; see below), nearly uniform across different types of galaxies residing in vastly different epochs. To illustrate this better, we plot the SFEs against the FIR luminosities in Figure 1 (*right*). The average SFEs in the various galaxy samples range from a low of 170 for the SMGs and LBGs to 250 for the LIRGs to 430 for the quasars and a high of 580 for the ULIRGs. The combined average of the SMGs, quasars, LBGs and U/LIRGs is 375 ± 42 (standard deviation = 327) $L_{\odot} (\text{K km s}^{-1} \text{pc}^2)^{-1}$. The average SFE of the SMGs is lower than the U/LIRGs by a factor of two, while a slightly higher average SFE seen in the quasars (and also the ULIRGs) is possibly attributable to higher dust temperature as a result of dust heating by the central AGN. Interestingly, the SFEs of the SMGs are more consistent with the widely separated LIRGs (and the LBGs and local galaxies) than the ULIRGs and quasars. We will return to this point in our discussion of the evolutionary status of the SMGs in §4.2. The SFE and L_{FIR} properties of the LBGs are also generally similar to the LIRGs, but this sample is currently limited to only two galaxies.

In U/LIRGs, the exact fraction of the AGN/starburst contribution to the FIR luminosity appears to depend on the source (Armus et al. 2007). Half of the fourteen U/LIRGs in our local sample show evidence for an AGN, but only in the two ULIRGs Mrk231 and Mrk273 is it possible that the AGN makes a significant contribution to the bolometric luminosity (Paper I, and references therein). This variation suggests that the scatter in the SFEs of U/LIRGs not only reflects the physical characteristics of each galaxy, but also the AGN heating of L_{FIR} in some sources. However, we mention the overall trend that the FIR output in local IRAS sources is dominated by starbursts and not AGN (Yun et al. 2001), as is evident from the robustness of the empirical radio-FIR correlation. In addition, while there is evidence from X-ray surveys that a good fraction of SMGs contain AGNs ($\sim 80\%$; Alexander et al. 2005), the energetic contribution of the AGN to the FIR output in most of the SMGs

appears to be minor (Pope et al. 2008; Valiante et al. 2007). Indeed, there is even evidence that most of the far-infrared luminosity in quasars comes from a central starburst (Lutz et al. 2007; Wang et al. 2007; Coppin et al. 2008), although there are exceptions (Weiss et al. 2007).

In Paper I, it was found that the relation between M_{H_2} (or $L'_{\text{CO}(3-2)}$) and L_{FIR} was not correlated with any significance, leading to an argument that the degree of gas concentration determines the level of star formation activity rather than the overall amount of molecular gas mass available in the galaxy. Due to large scatter in the SFEs of LIRGs (see Figure 1 (*right*)), the correlation indeed breaks down if we only consider the U/LIRGs in the fit. The LIRGs that have particularly low SFEs ($\lesssim 150$) are NGC 6240, Arp 193, VV 114, NGC 5257/8, and NGC 5331. Optically thin CO (3–2) is suggested from previous analysis on NGC 6240 (Iono et al. 2007), and therefore the CO (3–2) emission may be over-luminous with respect to other LIRGs with optically thick CO (3–2) emission. Although Arp 193 is apparently a late stage merger, VV 114, NGC 5257/8, and NGC 5331 show large nuclear separation suggestive of early stages of interaction. The SFEs of these galaxies are $93 - 117 L_{\odot} (\text{K km s}^{-1} \text{pc}^2)^{-1}$, which is a factor of three lower than the average of the entire sample. The factor of two lower average SFE seen in LIRGs (which have a mix of compact and widely separated sources) compared to ULIRGs (which are mainly compact) may suggest that the global SFE is lower in early to intermediate stage pre-coalescence mergers than in the centers of more advanced stage mergers, likely because the gas in intermediate stage mergers has not settled in a steady state in the rapidly evolving host stellar potential.

Finally, we note that the average SFE in local U/LIRGs is a factor of seven larger than $L_{\text{FIR}}/L'_{\text{CO}(2-1)} \sim 50$ found in two $z \sim 1.5$ BzK-color selected ULIRGs (Daddi et al. 2008). However, $L_{\text{FIR}}/L'_{\text{CO}(2-1)}$ may be significantly lower than $L_{\text{FIR}}/L'_{\text{CO}(3-2)}$ in the same galaxy owing to excitation effects, and future CO (3–2) observations of the same $z \sim 1.5$ BzK selected ULIRGs are necessary to compare the true CO (3–2) properties of molecular gas in ULIRGs at this redshift. Tacconi et al. (2008) have obtained upper limits to the CO (3–2) emission in three optically selected star forming galaxies similar to the BzK sample; however, the average lower limit to their SFE (> 90 , where we have estimated L_{FIR} from their measured star formation rates using the relation in Kennicutt 1998) implies that the local U/LIRGs have at most a factor of three times larger SFE. Upper limits to the CO (3–2) emission in 5 SMGs and 3 quasars (Greve et al. 2005; Coppin et al. 2008) give lower limits to their SFEs of > 160 to > 1000 . While most of these limits lie above the average SFE shown in Figure 1 (*right*), significantly more sensitive CO (3–2) observations of these sources would be needed to show conclusively that they deviate significantly in their properties from the detected SMGs and quasars.

3.2. Slope in the $L_{\text{FIR}} - L'_{\text{CO}}$ Relation

The CO (3–2) derived slope ($\alpha_{\text{CO}(3-2)} = 0.93 \pm 0.03$) in the $L_{\text{FIR}} - L'_{\text{CO}}$ relation is significantly steeper than a previous compilation which includes different excitation lines from local to high redshift sources (i.e. $\alpha_{\text{CO}} = 0.62 \pm 0.08$; Greve et al. 2005). This is expected because the molecular ISM in most of the SMGs is subthermally excited in CO transitions higher than $J = 4-3$ (Weiss et al. 2007b), and their sample of local U/LIRGs mainly consists of observations of $J = 1-0$. A study that investigates only the CO (3–2) line in local galaxies with FIR luminosities in the range $10^9-10^{12} L_{\odot}$ was conducted by Yao et al. (2003), where they find $\alpha_{\text{CO}(3-2)} = 0.70 \pm 0.04$. A more recent study (Narayanan et al. 2005) that relates the CO (3–2) to IR luminosity in a similar luminosity range suggests a near linear correlation ($\alpha_{\text{CO}(3-2)} = 1.08 \pm 0.07$). While there is variation in the slope among different studies, the slope between the CO (1–0) line and the FIR luminosity is even flatter ($\alpha_{\text{CO}(1-0)} = 0.58 \pm 0.07$; Yao et al. 2003) than that derived using the CO (3–2) emission alone. The relatively flat CO (1–0) slope suggests that the CO (1–0) derived SFE increases with increasing FIR luminosity (i.e.; Sanders et al. 1988a), and the molecular gas traced in CO (1–0) emission is not a linear tracer of star formation activity.

It has been demonstrated that the HCN emission, which is a higher density gas tracer than the commonly used CO (1–0) emission, produces a linear correlation with FIR luminosity ($\alpha_{\text{HCN}(1-0)} = 1.00 \pm 0.05$; Gao & Solomon 2004). Similar recent studies (Gao et al. 2007; Riechers et al. 2007; Gracia-Carpio et al. 2008) that include HCN observations from high redshift galaxies have shown, however, that $L_{\text{FIR}}/L'_{\text{HCN}}$ in the most distant galaxies is larger than the local sample by at least a factor of two, and the resultant fit between $L'_{\text{HCN}(1-0)}$ and L_{FIR} becomes flatter ($\alpha_{\text{HCN}(1-0)} = 0.81 \pm 0.06$; Gracia-Carpio et al. 2008) when high redshift galaxies are included. These new HCN results suggest that the dense gas fraction in bright high redshift galaxies is even higher than in the local IR bright galaxies.

In Figure 2, we show the different slopes (α_{mol}) plotted against the critical densities of the CO (1–0), CO (3–2) and HCN (1–0) transitions. We calculate the critical densities from $A_{ul}\gamma_{ul}^{-1}$ where A_{ul} is the Einstein A coefficient for the upper (u) to the lower (l) energy state and γ_{ul} is the corresponding collision rate obtained from the compilation of Schoier et al. (2005). A general trend that α_{mol} approaches unity for higher critical density tracers is evident from Figure 2.

The slope derived from CO (1–0) emission, $\alpha_{\text{CO}(1-0)}$, could be $\sim 2/3$ if a fixed fraction of gas converts to stars each free-fall time (Kennicutt 1998). From simple theoretical considerations, Krumholz & Thompson (2007) argue that, because the critical density of the CO (1–0) line is lower than the higher density tracers such as HCN, the CO (1–0) line traces the molecular gas that has densities close to the median density of a galaxy. On the other hand, molecules with high critical densities (such as the HCN (1–0) line) trace the ISM with much higher densities. In this case, $L_{\text{FIR}}/L'_{\text{HCN}(1-0)}$ does not depend strongly on the mean density of the galaxy, and therefore the slope derived from the HCN (1–0) measure-

ments (i.e. $\alpha_{\text{HCN}(1-0)}$) should be close to unity. They find, however, that the dependence of $L_{\text{FIR}}/L'_{\text{HCN}(1-0)}$ to the mean density becomes more significant at higher (10^{3-4} cm^{-3}) mean densities, suggesting that the slope can be flatter at the highest luminosity regime.

We plot the two theoretical predictions for $\alpha_{\text{CO}(1-0)}$ (dotted line) and $\alpha_{\text{HCN}(1-0)}$ (short dashed line) in Figure 2 as horizontal lines. The observations for these two emission lines are consistent with the theoretical predictions, and the new measurement by Gracia-Carpio et al. (2008) is also consistent with the prediction by Krumholz & Thompson (2007) that α_{HCN} is less than unity when galaxies with higher mean densities (represented by high redshift sources) are included in the fit. Our CO (3–2) measurements, as well as those measured by others, fall between the CO (1–0) and HCN (1–0) derived slopes, but the work by Krumholz & Thompson (2007) was limited to an isothermal case, and therefore could not investigate higher transition lines that are excited at higher temperatures such as the CO (3–2) line.

3.3. Molecular Excitation and Large Velocity Gradient Modeling

A theoretical investigation was performed by Narayanan et al. (2007b) to understand the dynamically evolving ISM of isolated and interacting galaxies. From their N-body/SPH simulations that include radiative transfer, they find that the total CO (3–2) luminosity has a mix of contribution from the dense cores (sites of star formation) and the more extended molecular gas that is subthermally excited. They argue that CO (3–2) and FIR luminosities are linearly correlated under the assumption that the gas density and SFR density are related by a Schmidt law (Schmidt 1959) index of 1.5. Further, a notable scatter is seen in the low luminosity end of their CO (3–2) – FIR luminosity relation, which is caused by line trapping of the CO (3–2) line by molecular gas surrounding the dense star forming cores and suggests that subthermally excited CO (3–2) gas can provide a substantial contribution to the overall $L'_{\text{CO}(3-2)}$.

In order to investigate the CO (3–2) excitation at different spatial scales, we derived the total (R_{total}) and peak (R_{peak}) CO (3–2) to CO (1–0) ratios in U/LIRGs using the CO (1–0) data available in the literature. The results are presented in Table 3. The average R_{total} is 0.48, ranging from 0.20 (Arp 55) to 1.25 (Arp 299W), whereas the average R_{peak} is 0.96, ranging from 0.36 (NGC 5257) to 3.21 (NGC 6240). On average, R_{peak} is two times higher than R_{total} . The two ratios are comparable for some of the compact sources such as IRAS 17208-0014, UGC 5101, Arp 299W, or NGC 5331N, but much larger in NGC 6240 (a factor of four larger). The lowest R_{peak} is derived in the brightest ULIRG in our sample, IRAS 17208-0014. The general inference of these results is that the CO (3–2) transition is nearly thermalized (in the optically thick limit) in the inner 1 – 3 kpc of the U/LIRGs, whereas the CO (3–2) transition is subthermally populated in the extended outskirts. This result is consistent with the theoretical prediction by Narayanan et al. (2007b), possibly suggesting that the scatter seen in the U/LIRGs in Figure 1 reflects

the excitation characteristics of each galaxy. Finally, we note that the *total* CO (3–2) emission in SMGs/quasars is nearly thermalized (Weiss et al. 2007b), and this could be the reason for the tighter correlation seen in the SMGs in Figure 1.

In order to obtain a better physical understanding of the observed variation in α_{mol} as well as the observed scatter in the SFEs, we constructed a series of Large Velocity Gradient (LVG) models (Goldreich & Kwan 1976) using the publicly available RADEX code (van der Tak et al. 2007). Figure 3 shows the expected flux as a function of H_2 density (see figure caption for the adopted input parameters). Three key arguments can be made from this figure. First, the rise in flux is nearly linear up to $\sim 10^4 \text{ cm}^{-3}$ for CO (3–2) and up to $\sim 10^5 \text{ cm}^{-3}$ for HCN (1–0), suggesting that these molecular transitions are good tracers of the density of the molecular medium up to these characteristic densities. The predicted flux beyond these characteristic values reaches an asymptotic value as the relevant lines become thermalized (i.e. $T_{ex} \sim T_{kinetic}$), thus predicting the gas densities from these lines alone becomes difficult in this regime. Second, the predicted flux of CO (3–2) and CO (1–0) lines cross at $\sim 10^4 \text{ cm}^{-3}$ (i.e. flux ratio of unity), and the line ratio is less than unity for densities below this critical value. Lastly, the temperature dependence of CO (3–2) is significant compared to the CO (1–0) line because the excitation temperature is higher in CO (3–2). At low densities ($n_{H_2} \sim 10^2 \text{ cm}^{-3}$), the observed CO (3–2) flux can vary by two orders of magnitude if the temperature of the ISM varies from galaxy to galaxy. Thus, at densities less than the critical density of the transition, collisional and radiative excitation both play key roles in populating the energy levels.

Under the assumptions adopted for the LVG model used here, the observed variation in α_{mol} can be explained in the following way. The low $\alpha_{CO(1-0)}$ likely reflects the nature of CO (1–0) emission as a low density tracer, and thus the higher density gas in U/LIRGs do not further increase the observed CO (1–0) flux, leading to the flattening of $\alpha_{CO(1-0)}$. The CO (3–2) emission is likely a tracer of higher density gas, but its flux is also sensitive to temperature, most notably in the low density end. Therefore, the relatively large scatter in the U/LIRGs and local galaxies in Figure 1 (*left*) could be explained by intrinsic variation in the average gas kinetic temperature and density, reflecting the physical characteristics of each galaxy. The results from LVG modeling are qualitatively consistent with the theoretical predictions by Krumholz & Thompson (2007) and Narayanan et al. (2007b).

Finally, we note that because the excitation of the CO (3–2) line could be sensitive to temperature, less temperature dependent higher density gas tracers such as HCN (1–0) or HCO^+ (Krumholz & Thompson 2007; Gracia-Carpio et al. 2008, but see Papadopoulos (2007) for a counter argument for the use of HCO^+) could be the better tracer of star formation in quiescent galaxies, although the gas must be dense ($n_{H_2} \sim 10^{5-6} \text{ cm}^{-3}$) enough to excite the HCN emission. These lines are also much weaker than CO lines and therefore harder to observe (see e.g. Figure 3). While HCN emission is often used a tracer of dense gas feeding star formation activity,

HCN emission from X-ray irradiated circumnuclear tori may become significant and therefore the HCN emission may be more pronounced towards AGN than starbursts in some cases (Kohno et al. 2001).

4. THE EVOLUTIONARY STATUS OF SUBMILLIMETER GALAXIES

4.1. CO (3–2) Source Size

In §3, we have shown evidence that the overall CO (3–2) luminosity is well correlated with the total dusty star formation traced in FIR luminosities. In this section, we extend this argument and assume that the large scale spatial distribution of CO (3–2) emission is also correlated with the extent of current star formation. To this end, we have plotted the CO (3–2) emitting diameter (in kpc) against the FIR luminosities in Figure 4. For the U/LIRGs, a trend is seen where the CO (3–2) size decreases as a function of FIR luminosity. The CO (3–2) size, however, can vary by an order of magnitude (0.3–3.1 kpc) for the LIRG population alone. In contrast, the ULIRGs are predominantly compact (0.4–1 kpc), and the large FIR luminosity seen in ULIRGs is likely related to this high central concentration of high density gas.

This trend immediately breaks down in SMGs where the derived CO (3–2) sizes (3–16 kpc) are roughly an order of magnitude larger than the ULIRGs. The average CO size for the SMGs (8 ± 2 kpc) is only a factor of two smaller than the average nuclear separation (15 ± 6 kpc) of the pre-coalescence LIRGs (e.g. VV 114, Arp 299; see also Figure 4). The three resolved quasars have source sizes (2–4 kpc) that are systematically smaller than the SMGs, but the sample size is too small for this trend to be conclusive. We caution that, although the SMGs/quasars are observed with the highest angular resolution achievable with existing interferometers, these sources are only marginally resolved, and the resultant source sizes should be treated as a conservative upper limit to any internal structure present in these galaxies. The upper limits for the unresolved SMGs and quasars (see Figure 4 (*right*)) do not place very useful limits on their intrinsic sizes, but are generally consistent with the conclusions drawn from the resolved sources.

These sizes show that the star forming regions in local ULIRGs are much more compact than those in SMGs. This result is an interesting contrast to the analysis by Bouché et al. (2007) where they find that the millimeter or CO size of the SMGs themselves are much more compact than the optical size of the UV or optically selected population at $z \sim 2$. The widely extended (as opposed to nuclear) star formation in SMGs was suggested previously using high resolution radio observations of spectroscopically identified SMGs by Chapman et al. (2004a) who find 70% of sources with size scale of 7 ± 1 kpc. More recently, Biggs & Ivison (2007) combined the radio emission data of SMGs obtained using Multi-Element Radio Linked Interferometer Network (MERLIN) and VLA in the $u-v$ plane, and found an average SMG source size of 5 kpc, which is in agreement with the results of Chapman et al. (2004a) and also the CO size measurements by Tacconi et al. (2006). Two-arcsecond resolution SMA 890 μm measurements (Iono et al. 2006b; Younger et al. 2007, 2008) of bright SMGs suggest source sizes of < 8 kpc, and new higher angular resolution SMA measurements suggest a smaller source size of ~ 5 kpc

(Younger et al. 2008). Thus, radio, CO, and submm observations all suggest that the size scale of the brightest SMGs are of order ~ 5 kpc, and this is a factor of 2 – 10 times larger than the CO (3–2) derived source sizes in U/LIRGs. The average size of the SMGs in our CO (3–2) selected sample (8 ± 2 kpc) is consistent with these numbers.

4.2. Merger Scenarios for SMGs and quasars

In Figure 5, we plot the CO (3–2) diameters as a function of the CO (3–2) FWHM. Roughly two thirds (18/26) of the source sizes for SMG/quasars are only upper limits constrained from the observations. It is evident from Figure 5 that even though the size scales of SMGs are comparable to the nuclear separation of the widely separated LIRGs (i.e. + sign in Figure 5), the FWHMs are on average 50% larger (and a factor of two larger than those of the ULIRGs).

The fact that both the average CO (3–2) sizes and the SFEs are similar for the SMGs and the local LIRGs suggests that they may be in a similar evolutionary state, e.g., that many of the SMGs are in fact early or intermediate rather than late stage mergers. Both the local ULIRGs (which are known to be advanced mergers) and the quasars are more compact (significantly so for the ULIRGs) and have SFEs that are a factor of three larger than those of the SMGs. In their analysis of several SMGs observed with the best angular resolution, Tacconi et al. (2008) also conclude that SMGs are major mergers in various evolutionary stages. They discuss three specific SMGs (two of which, SMM J163650+4057 and SMM J123707+6214, are included in our analysis) that each show two components separated by 8–25 kpc, which is more characteristic of earlier stage mergers of which local examples are Arp 299 and VV 114. Given that most SMGs are not observed at quite such high resolution, it remains possible that many SMGs could contain relatively compact CO reservoirs in two individual merging components, but not be sufficiently separated to be resolved with the existing data. However, this possibility would still be consistent with our interpretation of the SMGs as predominantly earlier stage mergers, as the resulting projected nuclear separation of SMGs would likely be as large as the widely separated LIRGs in our local sample.

In mergers of two comparable mass galaxies, the FWHM derived from the total CO (3–2) spectrum contains information pertaining to both galaxy rotation and encounter velocity. In principle, the encounter velocity of two comparable mass *field* galaxies in parabolic orbit is $\Delta V \sim \sqrt{2} V_c$ where ΔV and V_c are the encounter velocity and circular velocity, respectively. For local systems, ΔV amounts to ~ 300 km s⁻¹ at maximum. In reality, the observed ΔV is significantly smaller than this value, owing to, for example, projection and degeneracy in the merger phase, such as those seen in NGC 5331 ($\Delta V = 60$ km s⁻¹) or NGC 5257/8 ($\Delta V = 11$ km s⁻¹). At first glance, the broad CO (3–2) linewidths of SMGs (i.e. 600 km s⁻¹) argue against widely separated mergers. However, a simple analysis that assumes two equal mass field galaxies is likely inapplicable here because the brightest submillimeter sources are evidently embedded deep in the proto-cluster potential (Stevens et al. 2003; Greve et al. 2005). Thus, the encounter velocity of these

galaxies could be significantly larger than those of local field galaxies. For comparison, a similarly large velocity dispersion is observed in the galaxy members of the Virgo Cluster (Rubin, Waterman & Kenney 1999). The CO linewidth can trace the underlying stellar as well as the non-baryonic halo potential (Narayanan et al. 2008), and the suggested average stellar mass of SMGs ($2.5 \times 10^{11} M_\odot$; Borys et al. 2005) is significantly more massive than a typical field galaxy in the local universe (i.e. the Milky Way). Therefore, we suggest that the larger CO (3–2) FWHMs seen in SMGs are likely due to a combination of an underlying more massive dark matter potential and intrinsically more massive and gas-rich merger progenitors.

Analysis of numerical simulations (Greve & Sommer-Larsen 2008; Narayanan et al. 2006, 2007a, 2008) have found that the CO profile can display a variety of shapes owing to strong central outflows which could appear as secondary emission peaks in the CO spectra. These simulations further predict that the spectral characteristics have strong dependences on the sightline (i.e. the inclination of the source), as well as the mass of the underlying potential especially toward the latter stage of the evolution when the gas has settled in a disk (i.e. quasar phase). In addition, the simulated CO profile evolves as a function of merger age, where kinematic asymmetries are seen primarily in the pre-coalescence phase when the two galaxies have not yet merged. In contrast, the spectrum becomes closer to Gaussian as the molecular gas becomes virialized and a quiescent molecular disk is formed.

While some of their adopted assumptions may not be best suited for analyzing the observational data presented in this study, these simulation results provide important physical insight. The narrower CO (3–2) linewidths, and the dominance of Gaussian shapes in the quasar line profiles are consistent with the characteristics of a post-coalescence galaxy seen in simulations. In our limited sample of only three quasars, the size scale of quasars with robust size estimates are intermediate between the nuclear separation of pre-coalescence LIRGs and the very compact ULIRGs (see Figure 5). Given the factor of 10 larger average L_{FIR} in quasars compared to the local ULIRGs, we might naively expect the starburst region to be larger in the quasars, which could explain the size difference to within a factor of two. Alternatively, the quasar activity can begin in one of the progenitor galaxies earlier in the merger evolution than that predicted in simulations, and the abundance of CO (3–2) emitting molecular gas suggests intense concurrent starburst activity. It is also possible that CO (3–2) emission entrained in powerful AGN jets can lead to an apparent increase in the CO (3–2) size of quasars (Narayanan et al. 2006). Further, the observed narrower CO linewidths of quasars may simply be due to an intrinsically less massive quasar disk (Greve et al. 2005) or due to geometrical effects (Carilli & Wang 2006; Wu 2007) with quasars preferentially discovered in more face-on galaxies. It is, however, impossible to obtain a robust conclusion from our current compilation of data which is limited in sample size, sensitivity, and angular resolution.

Results from numerical simulations that include negative feedback from starbursts as well as the central AGN (Hopkins et al. 2005) suggest that SMGs and quasars are not in the same evolutionary stage, but linked through

dynamical evolution where the quasar activity becomes visible during the final stages of the coalescence. We have provided evidence in this paper that the CO (3–2) properties of many of the SMGs are consistent with the widely separated LIRGs in the local universe. A possible scenario suggested from these results is that SMGs are widely separated gas-rich mergers taking place near the centers of massive halos. Global disk-wide starburst activity in gas-rich high redshift mergers is also predicted theoretically by Mihos (2001). On the other hand, some of the CO (3–2) derived properties in quasars, such as size and SFE, are more consistent with ULIRGs than with LIRGs or SMGs. Overall, the data summarized here are broadly consistent with this evolution scenario.

Finally, we note that there is a selection effect in play. There are interacting/merging galaxies in the local universe that are not U/LIRGs; thus, the triggering of the U/LIRG activity also depends on the amount of pre-existing gas available in the merging pair. We also note that there are ULIRGs that are in the early stage of the interaction (Dinh-V-Trung et al. 2001), as well as LIRGs that are apparently isolated (i.e. NGC 1068). There is also a case like the $z = 4.7$ quasar – SMG pair BR1202–0725, in which two submm bright sources (one of which is a quasar, while the companion appears to harbor an obscured AGN, Iono et al. 2006c) are separated by a projected distance of 26 kpc. The true evolution, therefore, is much more complicated than we envision in these simple scenarios, and sensitive high resolution ALMA surveys of SMGs, quasars, as well as quiescent high redshift galaxies in a variety of evolutionary stages should reveal their true nature. Lastly, the gas consumption time for SMGs using the currently available fuel is estimated to be ~ 40 Myr (Greve et al. 2005), and this is significantly smaller than the typical major merger timescale of 1 Gyr. If the SMGs and quasars indeed represent some stage of the evolution of a merger with sustained starbursts, then the dense gas must be replenished continuously in order to maintain a continuous burst of star formation throughout the merger evolution.

5. SUMMARY

In this paper, we have presented a detailed comparison of the CO (3–2) emitting molecular gas between a local sample of luminous infrared galaxies (U/LIRGs) and a high redshift sample that comprises submm selected galaxies (SMGs), quasars, and two LBGs. The data for the local sample come from our recent Submillimeter Array survey of CO (3–2) emission in U/LIRGs while the CO (3–2) data for the high redshift population are obtained from the literature.

(1) We find that $L_{\text{CO}(3-2)}$ and L_{FIR} are correlated over five orders of magnitude, which suggests that the molecular gas traced in CO (3–2) emission is a robust tracer of star formation activity. The slope derived from the $\log L'_{\text{CO}(3-2)} - \log L_{\text{FIR}}$ relation is 0.93 ± 0.03 , and this near unity slope suggests that the efficiency of converting CO (3–2) emitting molecular gas to massive stars is, to within a factor of two, nearly uniform across different types of galaxies residing in different epochs. Within the local sample, the global star formation efficiency is lower in early to intermediate stage mergers than in the centers of more advanced stage mergers. SMGs show lower star

formation efficiencies that are comparable to those of the widely separated LIRGs.

(2) The slope derived for the $L'_{\text{CO}(3-2)} - L_{\text{FIR}}$ relation is significantly steeper than the slope derived from the same relation using the CO (1–0) emission. We show that this slope approaches unity for higher critical density tracers. Further, we show that the CO (3–2) emission in the central regions of U/LIRGs is, on average, nearly thermalized, whereas the outskirts are subthermally populated.

(3) From non-LTE LVG models as well as published merger evolution models that include radiative transfer, we argue that the CO (3–2) line is a fairly good tracer of star formation in SMGs, where the star forming gas density is high enough that the dependence on temperature is relatively low. In contrast, $L'_{\text{CO}(3-2)}$ can show significant scatter when the average gas density of the medium is lower than the critical density, which appears to occur more often in widely separated mergers in our sample. The scatter in the $L'_{\text{CO}(3-2)} - L_{\text{FIR}}$ relation, therefore, reflects the characteristics of the galaxy (temperature, density, and AGN heating of dust in some cases), but over a large range of luminosities, the CO (3–2) line appears to be a good probe of star formation.

(4) The CO (3–2) derived source sizes in U/LIRGs show an apparent trend that the brighter ULIRGs are systematically more compact than the less FIR bright LIRGs. The CO (3–2) sizes of the SMGs are on average an order of magnitude larger than the ULIRGs, and are comparable to the separation of the widely separated LIRGs in our sample. The three quasars with robust size constraints have source sizes that are somewhat smaller than the SMGs and a factor of two larger than the ULIRGs.

(5) The similarity in the CO (3–2) size and star formation efficiency between SMGs and LIRGs suggests that many of the SMGs studied here could be intermediate stage mergers. The SMG linewidths are, on average, much broader than many of the U/LIRGs, and we argue that the large encounter velocity likely arises from the massive halo potential in a proto-cluster environment. In contrast, quasars have smaller CO (3–2) sizes and linewidths, and a dominance of Gaussian shapes in the line profiles. These characteristics are consistent with those seen in post-coalescence galaxies in encounter simulations.

We thank the referee for detailed comments that improved the focus of this paper. DI would like to thank Ryohei Kawabe, Kotaro Kohno, Koichiro Nakanishi, Yoichi Tamura, Akira Endo, Fumi Egusa, Bunyo Hatsukade, Masahiro Sameshima, Kazuyuki Muraoka, Shinya Komugi, Desika Narayanan for useful discussion, and Thomas Greve for kindly providing tabulated data for the SMGs. The Submillimeter Array is a joint project between the Smithsonian Astrophysical Observatory and the Academia Sinica Institute of Astronomy and Astrophysics and is funded by the Smithsonian Institution and the Academia Sinica. This research has made use of the NASA/IPAC Extragalactic Database (NED) which is operated by the Jet Propulsion Laboratory, California Institute of Technology, under contract with the National

Aeronautics and Space Administration. This study was financially supported by MEXT Grant-in-Aid for Scientific Research on Priority Areas No. 15071202. C.D.W. acknowledges support by the Natural Science and Engi-

neering Research Council of Canada (NSERC). A.J.B. acknowledges support by National Science Foundation grant AST-0708653.

REFERENCES

- Aalto, S., Radford, S. J. E., Scoville, N. Z., & Sargent, A. I., 1997, *ApJ*, 475, L107
- Akritas, M. G., & Siebert, J., 1996, *MNRAS*, 278, 919
- Armus, L., Heckman, T., & Miley, G. 1987, *AJ*, 94, 831
- Armus et al., 2007, *ApJ*, 656, 148
- Alexander, D. M., Bauer, F. E., Chapman, S. C., Smail, I., Blain, A. W., Brandt, W. N., & Ivison, R. J., 2005, *ApJ*, 632, 736
- Barnes, J. E., & Hernquist, L., 1996, *ApJ*, 471, 115
- Baker, A. J., Tacconi, L. J., Genzel, R., Lehnert, M. D., & Lutz, D., 2004, *ApJ*, 604, 125
- Barger, A. J., Cowie, L. L., & Sanders, D. B., 1999, *ApJ*, 518, L5
- Barvainis, R., Lonsdale, C., & Antonucci, R., 1996, *AJ*, 111, 1431
- Barvainis, R., Alloin, D., Guilloteau, S., & Antonucci, R., 1998, *ApJ*, 492, 13
- Barvainis, R., & Ivison, R., 2002, *ApJ*, 571, 712
- Beelen, A., Cox, P., Pety, J., Carilli, C. L., Bertoldi, F., Momjian, E., Omont, A., Petitjean, P., & Petric, A. O., 2004, *A&A*, 423, 441
- Becker, R. H., White, R. L. & Helfand, D. J., 1995, *ApJ*, 450, 559
- Biggs, A. D., & Ivison, R. J., 2008, *MNRAS*, 385, 893
- Borys, C., Smail, I., Chapman, S. C., Blain, A. W., Alexander, D. M., & Ivison, R. J., 2005, *ApJ*, 635, 853
- Borys, C., et al., 2006, *ApJ*, 636, 134
- Bouché, N., et al., 2007, 671, 303
- Bryant P. M., & Scoville, N. Z., 1999, *AJ*, 117, 2632
- Carilli C., et al., 2004, *AJ*, 128, 997
- Carilli C. & Wang, 2006, *AJ*, 131, 2763
- Chapman, S. C., Smail, I., Windhorst, R., Muxlow, T., & Ivison, R. J., 2004, *ApJ*, 611, 732
- Chapman, S. C., Blain, A. W., Smail, I., & Ivison, R. J., 2004, *ApJ*, 622, 772
- Chapman, S. C., Blain, A. W., Smail, I., & Ivison, R. J., 2005, *ApJ*, 622, 772
- Condon, J. J., 1992, *ARA&A*, 30, 575
- Condon, J. J., Cotton, W. D., Greisen, E. W., Yin, Q. F., Perley, R. A., Taylor, G. B., & Broderick, J. J., 1998, *AJ*, 115, 1693
- Coppin, K. E. K., et al., 2007, *ApJ*, 665, 936
- Coppin, K. E. K., et al., 2008, *MNRAS*, 389, 45
- Cox, T. J., Jonsson, P., Primack, J. R., & Somerville, R. S., 2006, *MNRAS*, 373, 1013
- Daddi, E., Dannerbauer, H., Elbaz, D., Dickinson, M., Morrison, G., Stern, D., & Ravindranath, S. 2008, *ApJ*, 673, 21
- Downes, D., Solomon, P. M., Radford, S. J. E., 1995, *ApJ*, 453, 65
- Downes, D., & Solomon, P. M., 1998, *ApJ*, 507, 615
- Dunlop, J. S., McLure, R. J., Kukulka, M. J., Baum, S. A., O’Dea, C. P., & Hughes, D. H., 2003, *MNRAS*, 340, 1095
- Erb, Dawn K., Steidel, C. C., Shapley, A. E., Pettini, M., Reddy, N. A., & Adelberger, K. L., 2006, *ApJ*, 647, 128
- Efstathiou, A., Rowan-Robinson, M., & Siebenmorgen, R., 2000, *MNRAS*, 313, 734
- Frayser, D. T., Ivison, R. J., Scoville, N. Z., Yun, M. S., Evans, A. S., Smail, I., Blain, A. W., & Kneib, J. -P., 1998, *ApJ*, 506, 7
- Frayser, D. T., Ivison, R. J., Scoville, N. Z., Evans, A. S., Yun, M. S., Smail, I., Barger, A. J., Blain, A. W., & Kneib, J. -P., 1999, *ApJ*, 514, 13
- Gao, Y. & Solomon, P. M., 2004, *ApJ*, 606, 271
- Gao, Y., Carilli, C. L., Solomon, P. M., & Vanden Bout, P. A., 2007, *ApJ*, 660, L93
- Genzel, R., et al., 2006, *Nature*, 442, 786
- Goldreich, P., & Kwan, J., 1974, *ApJ*, 189, 441
- Gracia-Carpio, J., Garcia-Burillo, S., Planesas, P., Fuente, A., & Usero, A., 2008, *A&A*, 479, 703
- Greve, T. R., Ivison, R. J., Bertoldi, R., Stevens, J. A., Dunlop, J. S., Lutz, D., & Carilli, C. L., 2004, *MNRAS*, 354, 779
- Greve, T. R., et al. 2005, *MNRAS*, 359, 1165
- Greve, T. R. & Sommer-Larsen, J. 2008, *A&A*, 480, 335
- Genzel, R. et al., 1998, *ApJ*, 498, 579
- Genzel, R., Baker, A. J., Tacconi, L. J., Lutz, D., Cox, P., Guilloteau, S., & Omont, A., 2003, *ApJ*, 584, 633
- Guilloteau, S., Omont, A., Cox, P., McMahon, R. G., & Petitjean, P., 1999, *A&A*, 349, 363
- Hacking, P., Houck, J. R., & Condon, J. J., 1987, *ApJ*, 316, 15
- Hainline, L. J., Scoville, N. Z., Yun, M. S., Hawkins, D. W., Frayer, D. T., & Isaak, K. G., 2004, *ApJ*, 650, 614
- Hatsukade, B., et al., *PASJ* accepted (arXiv:0901.3388)
- Ho, P. T. P., Moran, J. M., & Lo, K. Y. 2004, *ApJ*, 616, L1
- Hopkins, P. F., Hernquist, L., Cox, T. J., Di Mateo, T., Martini, P., Robertson, B., & Springel, V., 2005, *ApJ*, 630, 705
- Iono D., Ho, P. T. P., Yun, M. S., Matsushita, S., Peck, A. B., & Sakamoto, K., 2004, *ApJ*, 616, L63
- Iono D., Yun, M. S., & Ho, P. T. P., 2005, *ApJS*, 158, 1
- Iono D., et al. 2006, *PASJ*, 58, 957
- Iono D., et al. 2006, *ApJ*, 640, L1
- Iono D., et al. 2006, *ApJ*, 645, L97
- Iono D., et al. 2007, *ApJ*, 659, 281
- Ivison, R. J., et al. 2002, *MNRAS*, 337, 1
- Kennicutt, R. C., 1998, *ApJ*, 498, 541
- Kim, D. -C., Veilleux, S., & Sanders, D. B., 1998, *ApJ*, 508, 627
- Kneib, J. -P., van der Werf, P. P., Knudsen, K. K., Smail, I., Blain, A. W., Frayer, D., Barnard, V., Ivison, R., 2004, *MNRAS*, 349, 1211
- Knudsen, K. K., van der Werf, P. P., & Jaffe, W., 2003, *A&A*, 411, 343
- Knudsen, K. K., Neri, R., Kneib, J. -P., & van der Werf, P. P., 2008, *A&A* in press (arXiv:0812.3409)
- Kohno, K., et al., 2001, *ASPC*, 249, 672
- Komugi, S., Kohno, K., Tosaki, T., Nakanishi, H., Onodera, S., Egusa, F., Sofue, Y., 2007, *PASJ*, 59, 55
- Krumholz, M. R., & Thompson, T. A., 2007, *ApJ*, 669, 289
- Lagache, G., Puget, J.-L., & Dole, H., 2005, *ARA&A*, 43, 727
- Lonsdale, C. J., Farrah, D., & Smith, H. E., 2006, "Astrophysics Update 2 - topical and timely reviews on astronomy and astrophysics". Ed. John W. Mason. Springer/Praxis books.
- Lutz, D., et al., 2007, *ApJ*, 661, L25
- Mauersberger, R., Henkel, C., Walsh, W., & Schulz, A., 1999, *ApJ*, 341, 256
- Motohara, K., Takata, T., Iwamuro, F., Eto, S., Shima, T., Mochida, D., Maihara, T., Nakanishi, K., & Kashikawa, N., 2005, *AJ*, 129, 53
- Mihos, J. C., & Hernquist, L., 1996, *ApJ*, 464, 641
- Mihos, J. C., 2001, *ASP Conference Series*, Vol. 230. Edited by Jose G. Funes, S. J. and Enrico Maria Corsini. San Francisco: Astronomical Society of the Pacific. ISBN: 1-58381-063-3, 2001, pp. 491-498
- Neri, R., Genzel, R., Ivison, R. J., Bertoldi, F., Blain, A. W., Chapman, S. C., Cox, P., Greve, T. R., Omont, A., & Frayer, D. T., 2003, *ApJ*, 597, L113
- Narayanan, D., Groppi, C. E., Kulesa, C. A., & Walker, C., 2005, *ApJ*, 630, 269
- Narayanan, D., Cox, T. J., Robertson, B., Dave, R., Di Matteo, T., Hernquist, L., Hopkins, P., Kulesa, C. A., & Walker, C., 2006, *ApJ*, 642, L107
- Narayanan, et al., 2008, *ApJS*, 176, 331
- Narayanan, D., Cox, T. J., Shirley, Y., Dave, R., Hernquist, L., & Walker, C. K., 2008, *ApJ*, 684, 996
- Narayanan, D., et al., 2008, *ApJS*, 174, 13
- Papadopoulos, P. P., 2007, *ApJ*, 656, 792
- Pope, A., Scott, D., Dickinson, M., Chary, R. R., Morrison, G., Borys, C., Sajina, A., Alexander, D. M., Daddi, E., Frayer, D., MacDonald, E., & Stern, D., 2006, *MNRAS*, 370, 1185
- Pope, A., et al., 2008, *ApJ*, 689, 127
- Priddey, R. S., Isaak, K. G., McMahon, R. G., & Omont, A., 2003, *MNRAS*, 339, 1183
- Riechers, D. A., Walter, F., Carilli, C., & Bertoldi, F., 2007, *ApJ*, 671, 13
- Robson, I., Priddey, R. S., Isaak, K. G., & McMahon, R. G., 2004, *MNRAS*, 351, L29
- Rowan-Robinson, M., et al., 1993, *MNRAS*, 261, 513
- Rubin, V. C., Waterman, A. H., & Kenney, J. D. P., 1999, *AJ*, 118, 236
- Sanchez, S. F., et al., 2004, *ApJ*, 614, 586

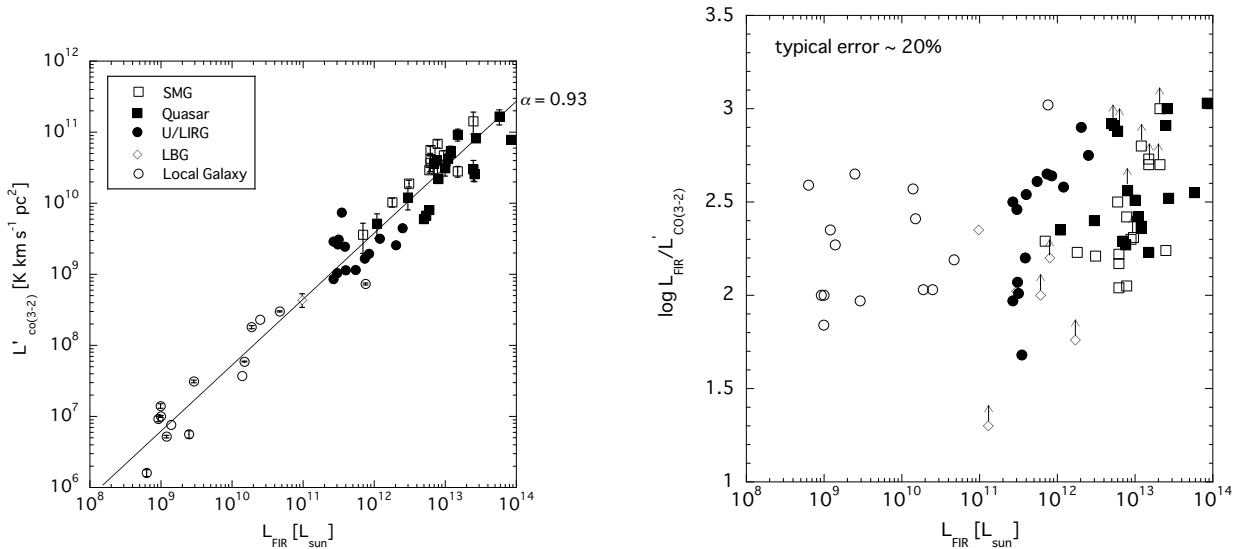


FIG. 1.— (*left*) The FIR Luminosity vs. $L'_{\text{CO}(3-2)}$ for all four populations. We have additionally plotted the same relation for the local galaxies. The fit to all of the points is shown in the solid line. (*right*) The L_{FIR} to $L'_{\text{CO}(3-2)}$ ratio vs. the FIR luminosity plotted in logarithmic scales. The symbols are the same as in *left*. We have additionally plotted the same relation for sources that were undetected in CO (3–2) using data published in Greve et al. (2005), Tacconi et al. (2008), Coppin et al. (2008) and Hatsukade et al. (2009). The FIR luminosities of the optically selected galaxies (classified as LBGs in this plot) in Tacconi et al. (2008) were estimated by taking the SFRs from Genzel et al. (2006) and Erb et al. (2006), and using the conversion given in Kennicutt (1998).

Sanders, D. B., Scoville, N. Z., Young, J. S., Soifer, B. T., Schloerb, F. P., Rice, W. L., & Danielson, G. E., 1986, *ApJ*, 305, 45
 Sanders, D. B., Soifer, B. T., Elias, J. H., Madore, B. F., Matthews, K., Neugebauer, G., & Scoville, N. Z., 1988, *ApJ*, 325, 74
 Sanders, D. B., Soifer, B. T., Scoville, N. Z., & Sargent, A. I., 1988, *ApJ*, 324, L55
 Sanders, D. B., Mazzarella, J. M., Kim, D. -C., Surace, J. A., Soifer, B. T., 2003, *AJ*, 126, 1607
 Sanders, D. B., & Mirabel, I. F. 1996, *ARA&A*, 34, 749
 Scoville, N. Z., Sanders, D. B., Sargent, A. I., Soifer, B. T., & Tinney, C. G., 1988, *ApJ*, 345, 25
 Scott, S. E., Fox, M. J., Dunlop, J. S., Serjeant, S., Peacock, J. A., Ivison, R. J., Oliver, S., Mann, R. G., Lawrence, A., & Efstathiou, A., 2002, *MNRAS*, 331, 817
 Schmidt, M., 1959, *ApJ*, 129, 243
 Sheth, K., Blain, A. W., Kneib, J.-P., Frayer, D. T., van der Werf, P. P., & Knudsen, K. K., 2004, *ApJ*, 614, 5
 Schoier, F. L., van der Tak, F. F. S., van Dishoeck, E. F., & Black, J. H., 2005, *A&A*, 432, 369
 Smail, I., Ivison, R. J., & Blain, A. W., 1997, *ApJ*, 490, L5
 Smail, I., Ivison, R. J., Blain, A. W., & Kneib, J. -P., 1998, *ApJ*, 507, L21
 Smail, I., Ivison, R. J., Blain, A. W., & Kneib, J. -P., 2002, *MNRAS*, 331, 495
 Smail, I., Smith, G. P., & Ivison, R. J. 2005, *ApJ*, 631, 121
 Solomon, P. M., & vanden Bout, P. A. 2005, *ARA&A*, 43, 677
 Springel, V., Yoshida, N., & White, S. D. M., 2001, *New Astronomy*, 6, 79
 Springel, V., Di Matteo, T., & Hernquist, L., 2005, *MNRAS*, 361, 776
 Stevens, J. A., et al., 2003, *Nature*, 425, 264
 Swinbank, A. M., Smail, I., Chapman, S. C., Blain, A. W., Ivison, R. J., & R., Keel, W. C. 2004, *ApJ*, 617, 64
 Tacconi, L. J., et al. 2006, *ApJ*, 640, 228
 Tacconi, L. J., et al. 2008, *ApJ*, 680, 246
 Toomre, A., & Toomre, J., 1972, *ApJ*, 178, 623
 Dinh-V-Trung, Lo, K. Y., Kim, D. C., Gao, Y., Grudel, R. A., 2001, *ApJ*, 556, 141

Valiante, E., Lutz, D., Sturm, E., Genzel, R., Tacconi, L. J., Lehnert, M. D., & Baker, A. J., 2007, *AJ*, 660, 1060
 Veilleux, S., Kim, D. -C., Peng, C. K., Ho, L. C., Tacconi, L. J., Dasyra, K. M., Genzel, R., Lutz, D., & Sanders, D. B., 2006, *ApJ*, 643, 707
 van der Tak, F. F. S., Black, J. H., Schoier, F. L., Jansen, D. J., & van Dishoeck, E. F., 2007, *A&A*, 468, 627
 Walter, F., Carilli, C., Bertoldi, F., Menten, K., Cox, P., Lo, K. Y., Fan, X., & Strauss, M. A., 2004, *ApJ*, 615L, 17
 Wang, R., et al., 2007, *AJ*, 134, 617
 Weiss, A., Henkel, C., Downes, D., & Walter, F., 2003, *A&A*, 409, 41
 Weiss, A., Downes, D., Neri, R., Walter, F., Henkel, C., Wilner, D. J., Wagg, J., Wiklind, T., 2007, *A&A*, 467, 955
 Weiss, A., Downes, D., Walter, F., & Henkel, C., 2007, “From Z-machines to ALMA”, *ASPC* 375
 White, R. L., Becker, R. H., Helfand, D. J., & Gregg, M. D., 1997, *ApJ*, 475, 479
 Wilson, C. D., et al., 2008, *ApJS*, 178, 189
 Wu, X. -B, 2007, *ApJ*, 657, 177
 Younger, J. D. et al., 2007, *ApJ*, 671, 1531
 Younger, J. D. et al., 2008, *MNRAS*, 387, 707
 Younger, J. D. et al., 2008b, *ApJ*, 688, 59
 Yao, L., Seaquist, E. R., Kuno, N., & Dunne, L., 2003, *ApJ*, 588, 771
 Yun, M. S., Scoville, N. Z., & Knop, R. A., 1994, *ApJ*, 430, L109
 Yun, M. S., Scoville, N. Z., Carrasco, J. J. & Blandford, R. D., 1997, *ApJ*, 479, L9
 Yun, M. S., Carilli, C. L., Kawabe, R., Tutui, Y., Kohno, K., & Ohta, K., 2000, *ApJ*, 528, 171
 Yun, M. S., Naveen, A. R., & Condon, J. J., 2001, *ApJ*, 554, 803
 Yun, M. S., & Carilli, C. L., 2002, *ApJ*, 568, 88
 Zakamska, N. L. et al., 2006, *AJ*, 132, 1496

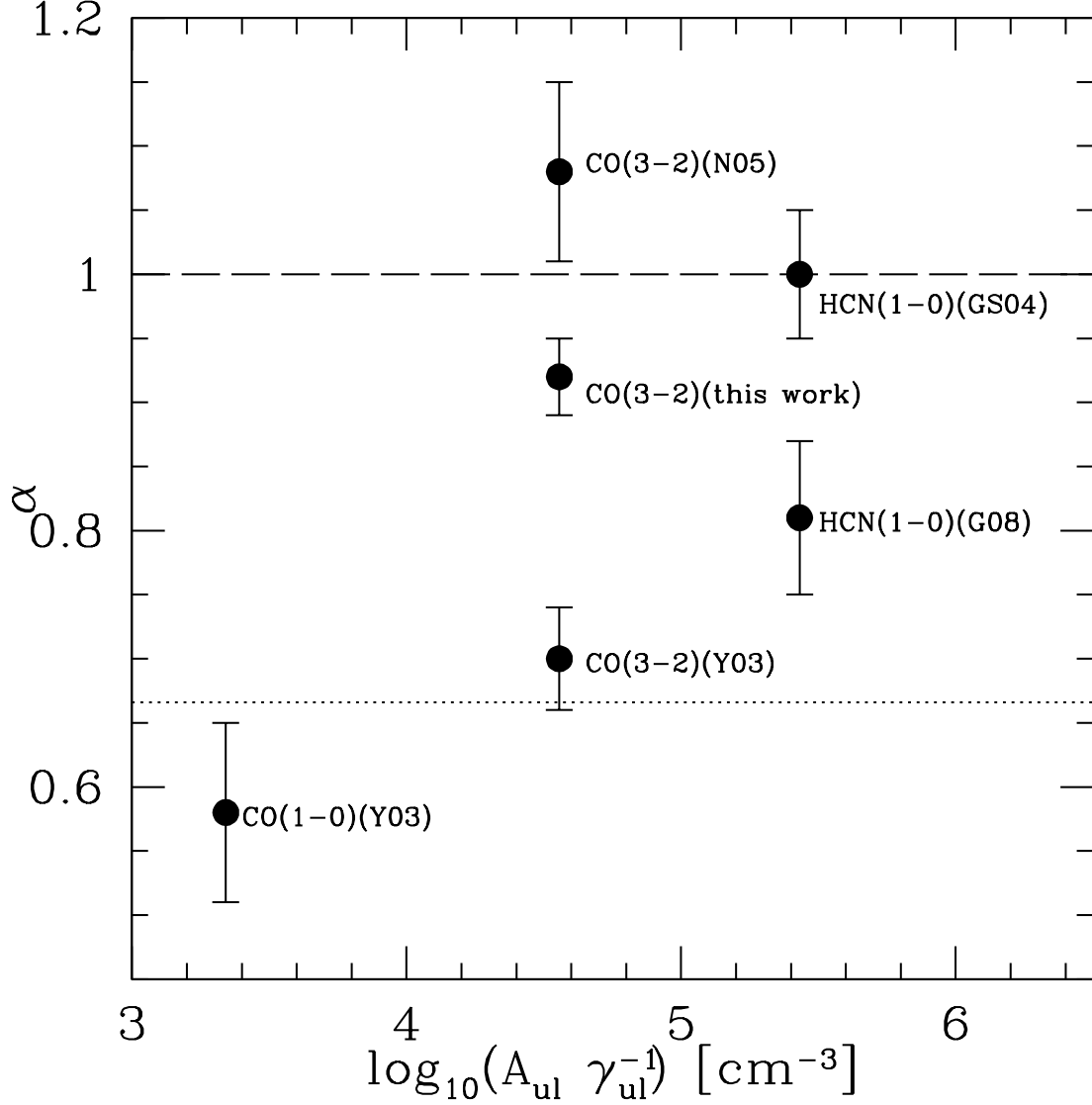


FIG. 2.— The index α_{mol} versus the critical density ($A_{ul}\gamma_{ul}^{-1}$) in the CO (1-0), CO (3-2), and the HCN (1-0) lines, where A_{ul} is the Einstein A coefficient in units of s^{-1} and γ_{ul}^{-1} is the collision rate coefficient in units of $\text{cm}^3 \text{s}^{-1}$. The collision rates (γ_{ul}) are obtained from Schoier et al. (2005), and the average of $T = 10, 20, 30, 50$ K are used. The dotted and short dashed lines represent the theoretical prediction for CO (1-0) and HCN (1-0) respectively from Krumholz & Thompson (2007). References: Yao et al. (2003) (Y03), Narayanan et al. (2005) (N05), Gao & Solomon (2004) (GS04), Gracia-Carpio et al. (2008) (G08).

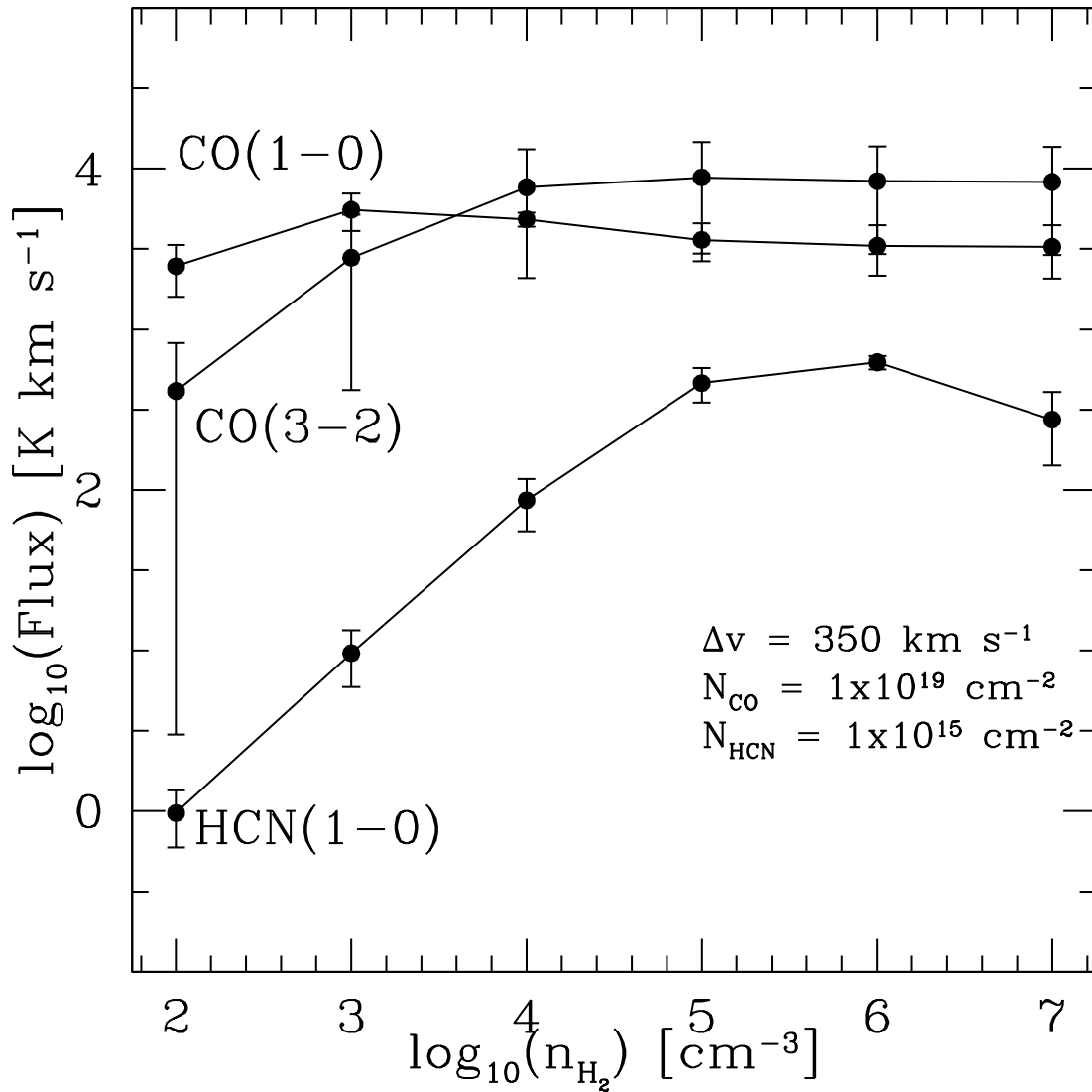


FIG. 3.— Large Velocity Gradient (LVG) modeling of the CO (1-0), CO (3-2) and HCN (1-0) lines. The average of the expected flux (in K km s^{-1}) is shown as a function of H_2 density. The error bars represent the range of possible fluxes when the kinetic temperature is varied from 20, 40, 60, 80, and 100K. The adopted LVG parameters are shown in the lower right. The column densities are motivated by the observational evidence of $N_{\text{H}_2} > 10^{23} \text{ cm}^{-2}$ in SMGs and U/LIRGs, and fractional abundance of CO and HCN to H_2 of $X_{\text{CO}} = 10^{-4}$ and $X_{\text{HCN}} = 10^{-8}$. We note that changing N_{H_2} will shift the absolute flux values for a given n_{H_2} , but the general shape remains the same. $\Delta V = 350 \text{ km s}^{-1}$ is the average CO (3-2) FWHM in U/LIRGs.

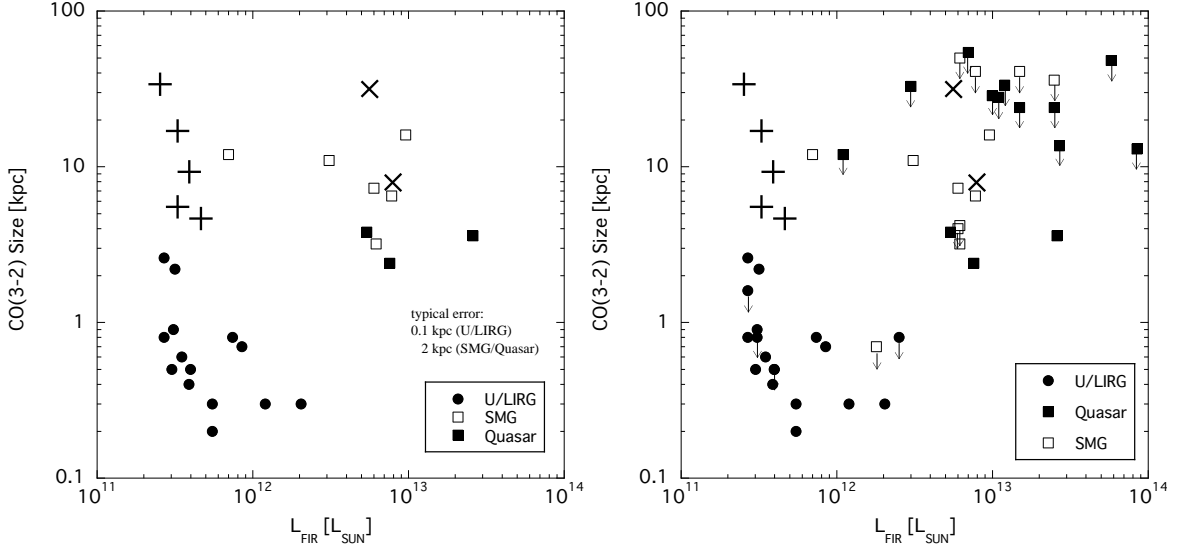


FIG. 4.— (*left*) The CO (3–2) size plotted against the FIR luminosities. The CO (3–2) minor axis was used for all sources. We note that some of the LIRGs (especially the low luminosity ones) are widely separated merging pairs, and here we have used the source sizes of each CO (3–2) component. Typical error bars are ~ 0.1 kpc for the U/LIRGs and ~ 2 kpc for the high redshift sources. We also plot the separation of the widely separated pairs for LIRGs (+) and SMGs (x). (*right*) Same as *left* but with the galaxies with only upper limits to the source size included for completeness.

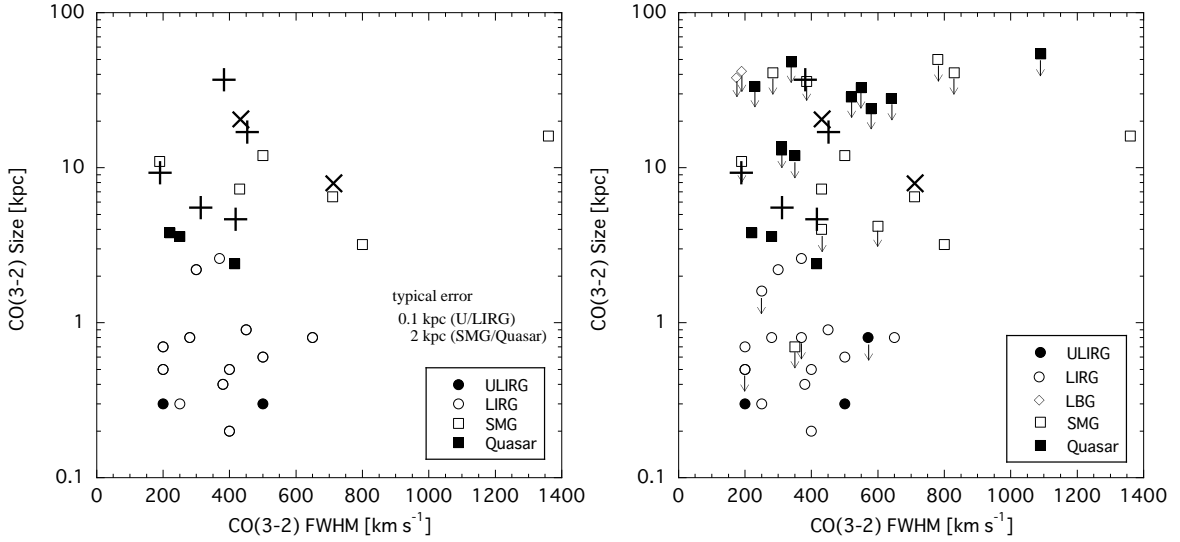


FIG. 5.— (*left*) The relation between source diameter (for SMGs, quasars, and LBGs) and the FWHM. (*right*) Same as *left* but with the galaxies with only upper limits to the source size included for completeness.

TABLE 1
SAMPLE PROPERTIES

Source	type	Distance ^a [Mpc or z]	Lensing Magnification	$\log L_{\text{FIR}}^{\text{b}}$ [L_{\odot}]	$\log L_{1.4}^{\text{c}}$ [W Hz^{-1}]	$S_{\text{submm}}^{\text{d}}$ [mJy]	Ref. ^e
U/LIRGs							
IRAS 17208-0014	ULIRG	189	...	12.41	23.55	48	1
Mrk 231	ULIRG	179	...	12.31	24.08	80	1
Mrk 273	ULIRG	166	...	12.08	23.68	56	1
IRAS 10565+2448	LIRG	191	...	11.93	23.40	15	1
UGC 5101	LIRG	174	...	11.87	23.79	37	1
Arp 299	LIRG	44 (4.7)	...	11.74	23.20	101	1
Arp 55	LIRG	173 (9.2)	...	11.60	23.12	26	1
Arp 193	LIRG	102	...	11.59	23.11	39	1
NGC 6240	LIRG	107 (0.5)	...	11.54	23.77	33	1
VV 114	LIRG	87 (5.6)	...	11.50	23.36	26	1
NGC 5331	LIRG	145 (18.3)	...	11.49	22.99	27	1
NGC 2623	LIRG	80	...	11.48	22.87	50	1
NGC 5257/8	LIRG	99 (38.4)	...	11.43	23.03	< 26/104	1
NGC 1614	LIRG	69	...	11.43	22.89	27	1
High Redshift Galaxies							
SMMJ02399-0136	SMG/QSO	2.808	2.5	12.98	24.57	9.6	2,3,4,5
SMMJ0443007+0210	SMG	2.509	4.4	12.25	23.10	1.6	4,5,6,7
SMMJ123549+6215	SMG	2.202	?	12.79	24.29	8.3	6,8
SMMJ123707+6214	SMG	2.49 (20)	?	12.78	24.19	9.9	6,8
SMMJ14011+0252	SMG	2.565	5 (or 25-30)	12.49	23.22	2.9	9,10
SMMJ16359+6612	SMG	2.517	22	11.85	...	0.7	14,15
SMMJ163650+4057	SMG	2.385	?	12.89	24.83	8.2	6,16
SMMJ163658+4105	SMG	2.452	1	12.79	24.48	10.7	6,16,17,18
SMMJ16371+4053	SMG	2.380	1	12.89	24.36	10.5	17,19
SMMJ22174+0015	SMG	3.099	1	12.79	24.39	6.3	17,20
MIPSJ1428	SMG	1.325	?	13.39	24.88	18.4	21,22
SMMJ163541+661144	SMG	3.187	1.7	13.18	...	6.0	39
SDSSJ1148+5251	QSO	6.419	?	13.41	25.15	7.8	23,24
RXJ0911.4+0551	QSO	2.796	22	12.06	< 23.95	1.2	25,26
LBQS1230+1627B	QSO	2.735	?	13.39	24.94	...	27
MG0414+0534	QSO	2.639	?	13.19	...	16.7	26,28
LBQS0018	QSO	2.620	?	13.09	< 25.57	17.2	29,30
VCVJ1409+5628	QSO	2.583	?	13.93	< 25.56	...	31
Cloverleaf	QSO	2.558	11	12.88	24.36	5.4	26,32
IRAS F10214+4724	QSO	2.286	17	12.73	23.23	2.9	33,34
SMMJ04135+1027	QSO/SMG	2.837	1.3	13.77	< 25.72	19.2	25,35
HS1002+4400	QSO	2.102	?	13.04	...	7.3 ^f	36
RXJ124913-055906	QSO	2.247	?	12.85	...	7.2	36
SMMJ131444+423814	QSO/SMG	2.556	?	12.48	...	3.0	36
VV96 J140955+562827	QSO	2.583	?	13.43	...	35.7 ^f	36
VV96 J154359+535903	QSO	2.370	?	13.00	...	12.7 ^f	36
HS1611+4719	QSO	2.396	?	13.08	...	15.4 ^f	36
MS 1512-cB58	LBG	2.727	31.8	10.99	22.85	...	37
J213512-010143	LBG	3.074	8	11.48	< 24.01	...	38
Average^g							
U/LIRGs		129 Mpc	...	11.74	23.37	49	
ULIRGs		178 Mpc	...	12.26	23.77	61	
LIRGs		116 Mpc	...	11.60	23.27	45	
SMGs		$z = 2.493$	5.3	12.76	24.19	7.8	
Quasars		$z = 2.782$	12.8	13.09	24.42	9.0	
LBGs		$z = 2.898$	19.9	11.23	22.85	...	

NOTE. — See Appendix of Paper I for the description of individual sources.

^aValues for U/LIRGs are given in D_L (Mpc) and the high redshift population are given in redshifts. For those sources that are resolved into two or more galaxies, the projected nuclear separation derived from 2MASS K-band images are shown in () in units of kpc.

^bValues are corrected for lensing if the lensing factor is known. See text for an explanation of how the values are derived. The FIR luminosity of cB58, and J213512 were obtained from Baker et al. (2004) and Coppin et al. (2007), respectively.

^cThe 1.4 GHz data were obtained from the NVSS (Condon et al. 1998) for the U/LIRGs, Smail et al. (2002) Chapman et al. (2005) for the SMGs, Carilli et al. (2004) White et al. (1997) Yun et al. (2000), Barvainis, Lonsdale & Antonucci (1996), for the quasars, and Becker et al. (1995) for the LBGs. Values are corrected for lensing if the lensing factor is known.

^dSMA 880 μm flux for the U/LIRGs (paper I). SCUBA 850 μm flux for the high redshift galaxies. Values are corrected for lensing magnification when the magnification factor is known.

^e1. Paper I, 2. Frayer et al. (1998), 3. Genzel et al. (2003), 4. Smail, Ivison, & Blain (1997), 5. Smail et al. (2002), 6. Tacconi et al. (2006), 7. Neri et al. (2003), 8. Chapman et al. (2005), 9. Frayer et al. (1999), 10. Smail et al. (1998), 11. Swinbank et al. (2004), 12. Motohara et al. (2005), 13. Smail, Smith & Ivison (2005), 14. Sheth et al. (2004), 15. Kneib et al. (2004), 16. Scott et al. (2002), 17. Greve et al. (2005), 18. Ivison et al. (2002), 19. Greve et al. (2004), 20. Barger, Cowie & Sanders (1999), 21. Iono et al. (2006a), 22. Borys et al. (2006), 23. Walter et al. (2004), 24. Robson et al. (2004), 25. Hainline et al. (2004), 26. Barvainis & Ivison (2002), 27. Guilloteau et al. (1999), 28. Barvainis et al. (1998), 29. Solomon & vanden Bout (2005), 30. Priddey et al. (2003), 31. Beelen et al. (2004), 32. Weiss et al. (2003), 33. Downes, Solomon & Radford (1995), 34. Rowan-Robinson et al. (1993), 35. Knudsen, van der Werf, & Jaffe (2003), 36. Coppin et al. (2008), 37. Baker et al. (2004), 38. Coppin et al. (2007), 39. Knudsen et al. (2008)

^fScaled the 1.2 mm flux in Coppin et al. (2008) to the 850 μm flux by assuming $\beta = 1.5$.

^gExcluding limits.

TABLE 2
CO (3–2) DERIVED PROPERTIES

Source	$L'_{\text{CO}(3-2)} \dagger$	Δ FWHM	Source Size ^a †	$(\frac{L_{\text{FIR}}}{L_{\text{CO}(3-2)}})^{\text{b}}$
U/LIRGs				
IRAS 17208-0014	4.5×10^9	570	$< 1.0 \times < 0.8$	564 (2.75)
Mrk 231	2.6×10^9	200	0.5×0.3	793 (2.90)
Mrk 273	3.2×10^9	500	0.4×0.3	378 (2.58)
IRAS 10565+2448	1.9×10^9	200	1.0×0.7	439 (2.64)
UGC 5101	1.7×10^9	650	1.1×0.8	448 (2.65)
Arp 299 (total) ^c	1.3×10^9	409 (2.61)
Arp 299E	8.4×10^8	400	0.3×0.2	...
Arp 299W	3.1×10^8	250	0.4×0.3	...
Arp 55 (total) ^c	1.1×10^9	349 (2.54)
Arp 55N	7.4×10^8	200	0.5×0.5	...
Arp 55S	4.1×10^8	200	$< 0.8 \times < 0.5$...
Arp 193	2.4×10^9	380	1.6×0.4	159 (2.20)
NGC 6240	7.4×10^9	500	0.9×0.6	47 (1.68)
VV 114	3.1×10^9	300	3.0×2.2	102 (2.01)
NGC 5331 (total) ^c	2.6×10^9	117 (2.07)
NGC 5331S	2.2×10^9	450	1.5×0.9	...
NGC 5331N	4.3×10^8	370	$< 1.9 \times < 0.8$...
NGC 2623	1.0×10^9	400	0.5×0.5	291 (2.46)
NGC 5257/8 (total) ^c	3.0×10^9	93 (1.97)
NGC 5257	6.7×10^8	250	$< 3.1 \times < 1.6^{\text{d}}$...
NGC 5258	2.2×10^9	370 ^e	$3.1 \times 2.6^{\text{d}}$...
NGC 1614	8.6×10^8	280	1.0×0.8	314 (2.50)
High Redshift Galaxies				
SMMJ02399-0136	4.7×10^{10}	1360 ± 50	16	203 (2.31)
SMMJ0443007+0210	1.0×10^{10}	350 ± 40	$< 3.1 \times < 0.7$	171 (2.23)
SMMJ123549+6215	4.2×10^{10}	600 ± 50	$< 4.2 (2.5)^{\text{f}}$	149 (2.17)
SMMJ123707+6214 (total)	2.9×10^{10}	206 (2.31)
SMMJ123707+6214SW	1.9×10^{10}	430 ± 60	7.3	...
SMMJ123707+6214NE	1.0×10^{10}	430 ± 60	< 4.0	...
SMMJ14011+0252	1.9×10^{10}	190 ± 11	11	164 (2.21)
SMMJ16359+6612	$3.6 \times 10^{9\text{g}}$	500 ± 100	$12 \times < 6$	196 (2.29)
SMMJ163650+4057	6.9×10^{10}	710 ± 50	$6.5 \times < 3.3$	113 (2.05)
SMMJ163658+4105	5.6×10^{10}	800 ± 50	3.2	110 (2.04)
SMMJ16371+4053	3.0×10^{10}	830 ± 130	$< 60 \times < 41$	262 (2.42)
SMMJ22174+0015	3.7×10^{10}	780 ± 100	$< 69 \times < 50$	166 (2.22)
MIPS-J1428	1.4×10^{11}	386 ± 104	< 36	173 (2.24)
SMMJ163541+661144	2.8×10^{10}	284 ± 50	$< 57 \times < 41$	536 (2.73)
SDSSJ1148+5251	2.6×10^{10}	280	$3.6 \times < 1.4$	1000 (3.00)
RXJ0911.4+0551	5.1×10^9	350 ± 60	$< 22 \times < 12$	222 (2.35)
LBQS1230+1627B	3.0×10^{10}	...	$< 48 \times < 24$	816 (2.91)
MG0414+0534	9.2×10^{10}	580	< 24	168 (2.23)
LBQS0018	5.4×10^{10}	163 ± 29	...	227 (2.36)
VCVJ1409+5628	7.9×10^{10}	311 ± 28	$< 20 \times < 13$	1084 (3.03)
Cloverleaf	4.0×10^{10}	416 ± 6	$< 20 \times < 12(2.4)$	188 (2.27)
IRASF10214+4724	6.7×10^9	220 ± 30	$3.8 \times < 2.5$	804 (2.91)
SMMJ04135+1027	1.7×10^{11}	340 ± 120	$< 96 \times < 48$	351 (2.55)
HS1002+4400	4.2×10^{10}	640 ± 160	$< 38 \times < 28$	262 (2.42)
RXJ124913-055906	3.6×10^{10}	1090 ± 340	$< 73 \times < 54$	194 (2.29)
SMMJ131444+423814	1.2×10^{10}	550 ± 220	$< 42 \times < 33$	250 (2.40)
VV96 J140955+562827	8.2×10^{10}	310 ± 30	$< 19 \times < 14$	329 (2.52)
VV96 J154359+535903	3.1×10^{10}	520 ± 140	$< 46 \times < 29$	323 (2.51)
HS1611+4719	5.1×10^{10}	230 ± 40	$< 41 \times < 33$	235 (2.37)
MS1512-cB58	4.4×10^8	174 ± 43	$< 65 \times < 38 (2.0)^{\text{h}}$	224 (2.35)
J213512-010143	2.9×10^9	190 ± 24	$< 48 \times < 42$	105 (2.02)
Averageⁱ				
U/LIRGs	$(2.6 \pm 0.5) \times 10^9$	360 ± 30	$(1.1 \times 0.8) \pm 0.3$	322 ± 56
ULIRGs	$(3.4 \pm 0.6) \times 10^9$	420 ± 110	$(0.5 \times 0.3) \pm 0.1$	578 ± 120
LIRGs	$(2.4 \pm 0.6) \times 10^9$	350 ± 30	$(1.3 \times 0.9) \pm 0.3$	252 ± 46
SMGs	$(4.4 \pm 1.1) \times 10^{10}$	590 ± 90	8.4 ± 1.9	194 ± 20
Quasars	$(5.0 \pm 1.0) \times 10^{10}$	430 ± 60	3.3 ± 0.4	430 ± 83
LBGs	$(1.6 \pm 1.2) \times 10^9$	180 ± 10	...	170 ± 60

NOTE. — Units are $[\text{K km s}^{-1} \text{ pc}^2]$ for $\log L'_{\text{CO}(3-2)}$, $[\text{km s}^{-1}]$ for Δ FWHM, [kpc] for source size, and $[L_{\odot} (\text{K km s}^{-1} \text{ pc}^{-2})^{-1}]$ for $L_{\text{FIR}}/L'_{\text{CO}(3-2)}$ in linear and logarithmic scales.

^a The deconvolved source size. Gaussian fits for IRAS 17208-0014, Arp 55S, NGC 5331N, NGC 5257 give only the upper limits shown. Sizes derived from CO transitions other than CO (3–2) are used for some of the high redshift sources. For high redshift sources with known luminosity magnification factors, we have scaled the CO size by the square root of the luminosity magnification assuming that the surface brightness is conserved during gravitational lensing.

TABLE 3
CO (3–2) – CO (1–0) RATIOS IN U/LIRGS

Source	R_{total}^a	R_{peak}^b	CO (1–0) Refs. ^c
IRAS 17208-0014	0.40	0.41	1
Mrk 231	0.35	0.82	1
Mrk 273	0.63	... ^d	1
IRAS 10565+2448	0.33	0.72	1
UGC 5101	0.46	0.48	2
Arp 299E	0.74	1.11	3
Arp 299W	1.25	1.30	3
Arp 55N	0.20	... ^e	4
Arp 55S		... ^e	4
Arp 193	0.61	< 1.26	1
NGC 6240	0.83	3.21	5
VV 114	0.25	0.49	6
NGC 5331S	0.30	0.55	7
NGC 5331N	0.50	0.50	7
NGC 2623	0.44	0.74	5
NGC 5257	0.21	0.36	7
NGC 5258	0.38	1.06	7
NGC 1614	0.35	... ^f	8
average	0.48	0.93	

^a The CO (3–2) to CO (1–0) flux ratio using the total luminosities.

^b The CO (3–2) to CO (1–0) flux ratios using the peak fluxes. The peak fluxes were derived after convolving the CO (3–2) maps to the lower resolution CO (1–0) maps, except for Arp 193 where the CO (1–0) map has higher angular resolution than the CO (3–2) map. The peak CO (1–0) fluxes were obtained from the images published in the references. These ratios trace the inner 1–3 kpc of the galaxies.

^c 1. Downes & Solomon (1998), 2. Genzel et al. (1998), 3. Aalto et al. (1997) 4. Sanders et al. (1988b), 5. Bryant & Scoville (1999), 6. Yun et al. (1994) 7. Iono, Yun & Ho (2005), 8. Scoville et al. (1989)

^d There appear to be inconsistencies in the published values of Mrk 273 in Fig. 15 of Downes & Solomon (1998). The peak flux level ($\sim 144 \text{ Jy km s}^{-1} \text{ beam}^{-1}$) exceeds the total flux (78 Jy km s^{-1}) given in the same paper.

^e Although the CO (1–0) contours are shown overlaid on an optical image, the contour levels were not explicitly given in Sanders et al. (1988b).

^f NGC 1614 is unresolved in this paper.